The Astrophysical Journal, 700:783–790, 2009 July 20 doi:10.1088/0004-637X/700/1/783

INDEPENDENT CONFIRMATION AND REFINED PARAMETERS OF THE HOT JUPITER XO-5b*

A. Pál[1,2,3], G. Á. Bakos[1,8], J. Fernandez[1], B. Sipőcz[1,2], G. Torres[1], D. W. Latham[1], Géza Kovács[3], R. W. Noyes[1], G. W. Marcy[4], D. A. Fischer[5], R. P. Butler[6], D. D. Sasselov[1], G. A. Esquerdo[1], A. Shporer[7], T. Mazeh[7], R. P. Stefanik[1], and H. Isaacson[5]

[1] Harvard-Smithsonian Center for Astrophysics, Cambridge, MA, USA; apal@szofi.net
[2] Department of Astronomy, Eötvös Loránd University, Budapest, Hungary
[3] Konkoly Observatory, Budapest, Hungary
[4] Department of Astronomy, University of California, Berkeley, CA, USA
[5] Department of Physics and Astronomy, San Francisco State University, San Francisco, CA, USA
[6] Department of Terrestrial Magnetism, Carnegie Institute of Washington, DC, USA
[7] Wise Observatory, Tel Aviv University, Tel Aviv 69978, Israel
Received 2008 October 1; accepted 2009 May 15; published 2009 July 6

ABSTRACT

We present HATNet observations of XO-5b, confirming its planetary nature based on evidence beyond that described in the announcement of Burke et al., namely, the lack of significant correlation between spectral bisector variations and orbital phase. In addition, using extensive spectroscopic measurements spanning multiple seasons, we investigate the relatively large scatter in the spectral line bisectors. We also examine possible blended stellar configurations (hierarchical triples, chance alignments) that can mimic the planet signals, and we are able to show that none are consistent with the sum of all the data. The analysis of the S activity index shows no significant stellar activity. Our results for the planet parameters are consistent with values in Burke et al., and we refine both the stellar and the planetary parameters using our data. XO-5b orbits a slightly evolved, late G type star with mass $M_\star = 0.88 \pm 0.03\ M_\odot$, radius $R_\star = 1.08 \pm 0.04\ R_\odot$, and metallicity close to solar. The planetary mass and radius are $1.059 \pm 0.028\ M_J$ and $1.109 \pm 0.050\ R_J$, respectively, corresponding to a mean density of $0.96^{+0.14}_{-0.11}$ g cm^{-3}. The ephemeris for the orbit is $P = 4.187757 \pm 0.000011$ days, $E = 2454552.67168 \pm 0.00029$ (BJD) with transit duration of 0.1307 ± 0.0013 days. By measuring four individual transit centers, we found no signs for transit timing variations. The planet XO-5b is notable for its anomalously high Safronov number and has a high surface gravity when compared to other transiting exoplanets with similar period.

Key words: planetary systems – stars: individual (XO-5, GSC 02959-00729) – techniques: spectroscopic

1. INTRODUCTION

There are numerous dedicated transit searches surveying the sky for extrasolar planets that periodically transit across the face of their host star. Among the wide angle searches, those presenting discoveries have been TrES (Brown & Charbonneau 2000; Dunham et al. 2004; Alonso et al. 2004; Mandushev et al. 2007), XO (McCullough et al. 2005; Burke et al. 2007), HATNet (Bakos et al. 2002, 2004), and SuperWASP (Street et al. 2003; Pollacco et al. 2006; Cameron et al. 2007). The initial high hope of finding hundreds of such planets (Horne 2001) was followed by five years of poor harvest, and a steep learning curve for these, and many other projects. In retrospect we now understand that several important factors had initially been underestimated, such as the need for dedicated telescope time, optimal precision, stable instrumentation, low systematic noise, the number of false positives (Brown 2003), optimal follow-up strategy, and access to high precision spectroscopic instruments. The last year showed an exponential rise in announcements,[9] indicating that these dedicated efforts have started bearing fruit. In fact, they have reached a success rate such that the same object is occasionally independently found and announced by different groups (WASP-11b: West et al. (2008) = HAT-P-10b: Bakos et al. 2009). Such scenarios are not necessarily duplication of effort. It is reassuring that completely independent discoveries, follow-up observations, and analyses lead to similar parameters. They also provide an opportunity for joint analysis of all data sets. Here we report on a similar case, the confirmation of the planetary nature of the transiting object XO-5b, announced by Burke et al. (2008). The present paper provides not only strong new evidence supporting the planetary nature of the object, but also improved physical properties that aid in the comparison with theories of planet structure and formation. In Section 2, we describe the details of the photometric detection. The follow-up observations, including the discussion of the bisector span measurements are presented in Section 3. The subsequent steps of the analysis in order to characterize the star, orbit, and the planet are discussed in Section 5.

2. PHOTOMETRIC DETECTION

Two telescopes of the HATNet project, namely HAT-6, stationed at Fred Lawrence Whipple Observatory (FLWO; $\lambda = 111^\circ$ W), and HAT-9, located on the rooftop of the Submillimeter Array control building at Mauna Kea, Hawaii ($\lambda = 155^\circ$ W), were used to observe HATNet field "G176" ($\alpha = 07^h28^m$, $\delta = +37^\circ30'$) on a nightly basis between 2004 November 26 and 2005 May 9. Altogether we acquired with these telescopes 2640 and 4280 frames, respectively, with exposures of 5 minutes.

A number of candidates have emerged from this field and have been subjected to intense follow-up by larger instruments (Section 3). One candidate has become the transiting planet we call HAT-P-9b (Shporer et al. 2009). Another candidate

* Based in part on observations obtained at the W. M. Keck Observatory, which is operated by the University of California and the California Institute of Technology. Keck time has been granted by NOAO and NASA (programs N162Hr, N128Hr, and A264Hr).
[8] NSF Fellow.
[9] http://www.oklo.org, http://www.exoplanet.eu

internally labeled as HTR176-002 has received extensive follow-up over the past two years. However, the large scatter in the spectral line bisectors, and their tentative correlation with orbital phase discouraged us from early announcement, and motivated us to pursue it further. Subsequently, HTR176-002 was announced as XO-5b by the XO group in 2007 May (Burke et al. 2008, hereafter B08). Nevertheless, we present here our results since they provide independent confirmation and also refine most of the parameters.

By chance, XO-5 happens to fall at the edge of field "G176" which overlaps with field "G177" ($\alpha = 08^{\rm h}00^{\rm m}$, $\delta = +37^\circ30'$). This field has been observed by the HATNet telescope HAT-7 and by the WHAT telescope at Wise Observatory, Israel (Shporer et al. 2006). Using these telescopes we collected 5440 and 1930 frames, respectively. Altogether we obtained ~14,290 frames with photometric information on XO-5—an unusually rich data set compared to data available for a typical HATNet transit candidate.

The frames from field "G176" were processed and analyzed as described, e.g., in Bakos et al. (2007). The light curves from this field were corrected for trends using the method of External Parameter Decorrelation (EPD; see Bakos et al. 2009), and the Trend Filtering Algorithm (TFA; Kovács et al. 2005). The light curves were then searched for periodic box-like signals using the Box Least Squares algorithm of Kovács et al. (2002). We detected a significant dip in the light curve of the $I \approx 12.17$ mag star GSC 02959-00729 (also known as 2MASS 07465196+3905404; $\alpha = 7^{\rm h}46^{\rm m}51\overset{\rm s}{.}97$, $\delta = +39^\circ05'40\overset{''}{.}5$; J2000), with a depth of ~12 mmag. The period of the signal was $P = 4.1878$ days, while the relative duration (first to last contact) of the transit events was $q \approx 0.027$, which is equivalent to a total duration of $Pq \approx 2.6$ hr (see Figure 1(a)).

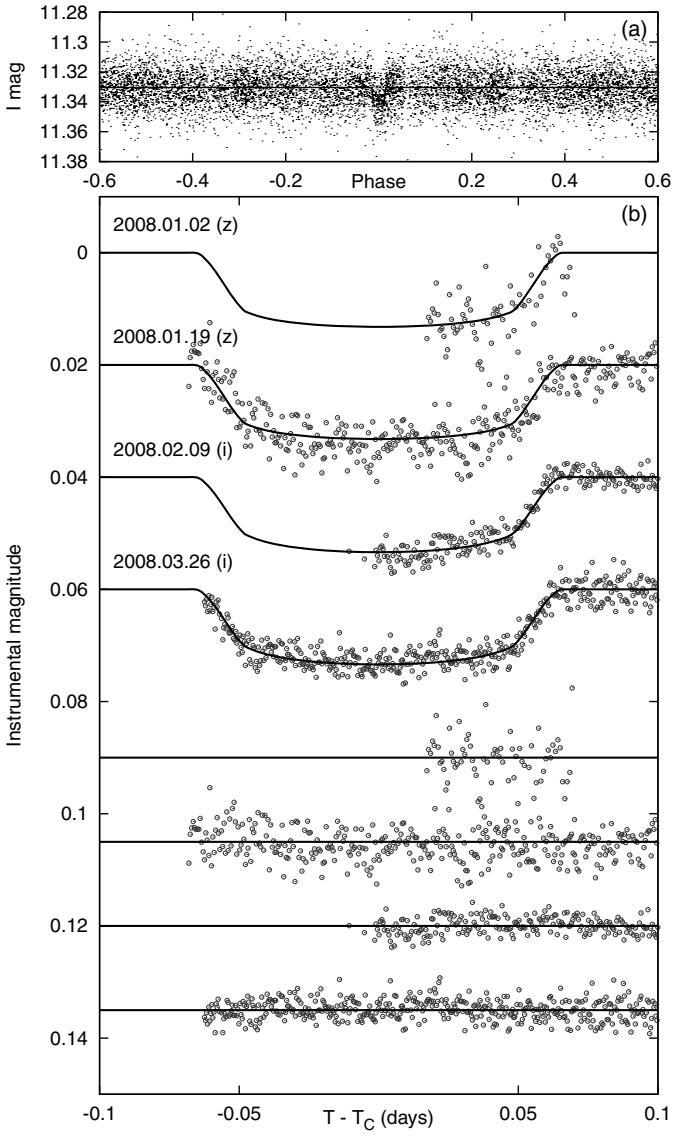

Figure 1. (a) Light curve of XO-5 with all 14,290 points taken in the *I* band, by the telescopes HAT-6, HAT-7, HAT-9, and WHAT. The light curve is folded with the period of $P = 4.187757 \pm 0.000011$ days (which is the result of the fit described in Section 5). The superimposed curve shows the best fit model, neglecting limb darkening. (b) Unbinned instrumental Sloan *z* band and *i* band follow-up transit photometry light curves acquired with KeplerCam on the FLWO 1.2 m telescope on 2008 January 2 ($N_{\rm tr} = 0$, *z* band), January 19 ($N_{\rm tr} = 4$, *z* band), February 9 ($N_{\rm tr} = 9$, *i* band) and March 26 ($N_{\rm tr} = 20$, *i* band). Superimposed are our best-fit transit models (Section 5).

3. FOLLOW-UP OBSERVATIONS

3.1. Reconnaissance Spectroscopy

In order to exclude the possibility of a false planetary detection, due to the misinterpretation of a transit-like signal caused by another astrophysical scenario (such as an F + M dwarf system), we observed the candidate HTR176-002 with the CfA Digital Speedometer (Latham 1992) on the FLWO 1.5 m Tillinghast reflector. We acquired four spectra between 2007 January and March, each with an individual precision of 0.5 km s^{-1}. The observations showed a mean radial velocity (RV) of $\gamma = -10.6$ km s^{-1} with an rms of 0.3 km s^{-1}, therefore ruling out a low-mass stellar companion (but not a triple system), which would cause significantly higher RV variations. The spectroscopy also yielded an estimate for the projected rotational velocity and surface gravity of the star.

3.2. High S/N Spectroscopy and Subsequent Analysis

We obtained high resolution and high signal-to-noise spectra with the Keck-I telescope and High Resolution Echelle Spectrometer (HIRES) instrument (Vogt et al. 1994). We acquired 17 exposures with the iodine cell, and an additional iodine-free "template." The measurements were made between 2007 March 27 and 2008 May 17. The purpose of these observations was threefold: (1) to obtain high precision RV measurements; (2) to characterize the stellar properties; and (3) to check for spectral line bisector variations as an indication of blends. These steps are discussed in the following paragraphs.

As regards measuring the RV variations, the superimposed dense forest of I_2 absorption lines enables us to obtain an accurate wavelength shift compared to the template observation (Marcy & Butler 1992; Butler et al. 1996). The final RV measurements and their errors are listed in Table 1. The folded data, with our best fit (see Section 5) superimposed, are plotted in Figure 2, upper panel.

The stellar atmosphere parameters were determined using the iodine-free template spectrum. The spectral modeling was performed using the Spectroscopy Made Easy (SME) software (Valenti & Piskunov 1996), with wavelength ranges and atomic line data as described by Valenti & Fischer (2005). We obtained the following *initial* values: effective temperature $T_{\rm eff} = 5505 \pm 70$ K, surface gravity $\log g_\star = 4.61 \pm 0.10$ (cgs), iron abundance [Fe/H] $= +0.16 \pm 0.06$, and projected rotational velocity $v \sin i = 0.7 \pm 0.5$ km s^{-1}.

Table 1
Relative Radial Velocity, Bisector Span and Stellar Activity (S) Measurements of XO-5

BJD (2, 454, 000+)	RV (m s^{-1})	σ_{RV} (m s^{-1})	Bisec (m s^{-1})	σ_{Bisec} (m s^{-1})	S
186.94763	269.14	3.21	41.75	33.63	0.1620
187.94425	...	...	35.88	35.33	0.1530
187.95384	226.59	3.08	−0.36	47.48	0.1598
188.95403	33.07	2.79	20.77	42.04	0.1589
216.76639	294.36	2.70	81.43	20.90	0.1549
247.80697	0.00	3.37	−30.10	45.47	0.1876
248.77938	76.84	3.83	−34.80	48.41	0.1855
249.78531	268.26	3.36	12.13	36.59	0.1548
251.78153	5.41	3.75	−110.60	64.06	0.1459
428.02826	8.16	3.02	100.80	15.23	0.1543
430.12240	301.03	3.71	94.90	16.46	0.1549
455.97787	222.99	3.41	93.23	16.03	0.1505
547.92199	224.82	7.25	... [a]	... [a]	0.1577
548.81658	79.96	3.08	82.68	22.18	0.1595
548.89652	65.98	2.84	73.55	24.33	0.1576
602.74168	193.74	2.61	59.89	25.39	0.1578
603.74268	15.18	2.83	60.49	25.44	0.1604

Note.
[a] This spectrum turned out to be severely contaminated by moonlight; however, the corresponding RV is unaffected.

3.3. Photometric Follow-up Observations

We obtained follow-up photometric observations on four nights using the KeplerCam CCD on the FLWO 1.2 m telescope through Sloan z and i bands. The observations were performed on 2008 January 2 (partial transit), January 19 (full transit), February 9 (partial) and March 26 (full), with the total number of object frames being 114, 428, 268, and 521, respectively. The integration times used at these nights were 45, 30, 30, and 15 s, respectively, while the readout and storage required an additional ∼12 s per frame. The typical rms of the follow-up light curves was 2 mmag at the above cadence.

We performed aperture photometry on the calibrated frames, using an aperture series that ensures optimal flux extraction. Details on the astrometry (see Pál & Bakos 2006), photometry, decorrelation for trends, etc., have been discussed in, e.g., Bakos et al. (2007). The light curves are plotted in the lower panel of Figure 1, superimposed with the best-fit transit light curve model (see Section 5).

4. BLEND ANALYSIS

A stellar eclipsing binary that is unresolved from a bright source would manifest itself as a blended system with shallow photometric transits, and with RV variations that are of the same order of magnitude as one can expect from a planetary system (e.g., Queloz et al. 2001). We investigated whether such a blend is a feasible physical model for HTR176-002 in two ways: by examining the spectral line bisectors and with a detailed modeling of the light curve under various possible blend scenarios.

For a blended eclipsing binary, in addition to the decrease in the observed RV amplitude, the spectral lines would be distorted, as quantified by the "bisector spans" (see Torres et al. 2005, 2007). If the bisector span variations correlate with the orbital phase, or the magnitude of these variations is comparable with the RV amplitude, then the system is likely to be a false positive (hierarchical triple or chance alignment with a background binary) rather than a single star with a planetary

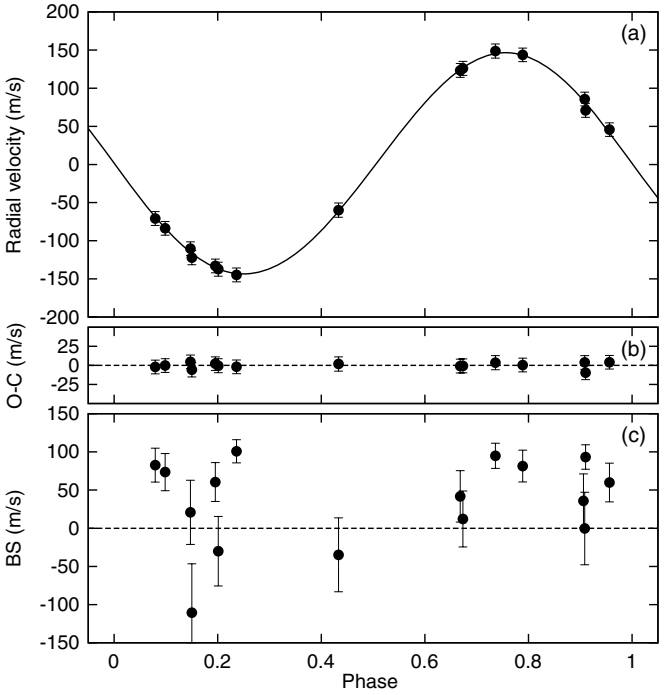

Figure 2. (a) RV measurements from Keck for XO-5, along with our orbital fit (see Section 5). The center-of-mass velocity γ and the correlation correction for the bisector span variations has been subtracted. (b) Phased residuals after subtracting the orbital fit (also see Section 5). The rms variation of the residuals is about 4.6 m s^{-1}. (c) Bisector spans (BS) for 16 of the Keck spectra (including the iodine-free template). Note that the scales of the panels are the same.

companion. In order to rule this out we derived the bisector spans by cross-correlating the iodine-free ranges of the obtained spectra against a synthetic template spectrum. We found that the standard deviation of the bisector spans is approximately ∼60 m s^{-1}, which is comparable to the magnitude of the RV variation itself ($K = 144.9 \pm 2.0$ m s^{-1}; see Table 3). The large bisector variations discouraged us from publication even after the first full transit follow-up light curve was obtained in January 2008, and we continued acquiring high resolution spectroscopy to establish whether there is any significant correlation between the bisectors and the orbital phase (or equivalently, with the actual RV values). In Figure 3, we display our measurements of the bisector spans as the function of both the RV and the RV residuals from the best fit.[10] There is no statistically significant correlation between the velocities and bisector variations, as would be expected for a blend. However, there is apparently a correlation between the RV *residuals* and the bisector spans. This could be due to activity on the star (e.g., spottedness), where the activity (if periodic) causes both RV and bisector variations, but in a way that is not commensurate with the orbital period of the companion. We exploit this correlation in the joint analysis of the RV and photometric data (see Section 5) where we show that the unbiased residual of the RV signal can be significantly decreased with the inclusion of an additional term proportional to the bisector spans.

In order to rule out or confirm the importance of the stellar activity, we computed the Ca II emission index S (Noyes et al. 1984). The derived indices are also shown in Table 1. We found that the mean value of $S = 0.16 \pm 0.02$ is moderately low, and

[10] As we will discuss later, our finally accepted best-fit values were derived by including a decorrelation factor against this bisector span correlation. In the plot the RV residuals are shown before subtracting this correlation term.

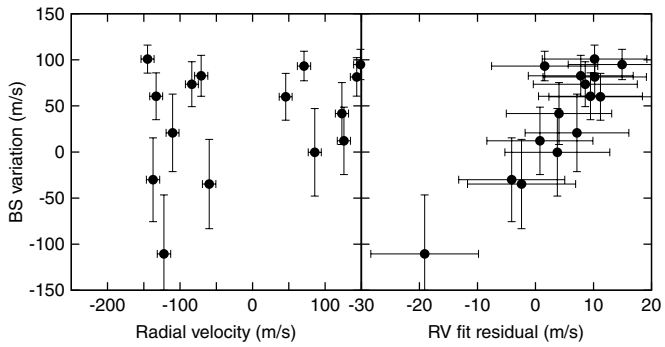

Figure 3. Bisector span variations as a function of the RV (left panel) and RV fit residual (right panel). The right panel shows the fit residuals when the correlation term was not included in the fit. Note that on the graphs the horizontal scales are not the same.

the correlations between the values of S and the RV data or RV fit residuals are negligible (see also Section 5.1).

As a further way of assessing the true nature of the candidate, we investigated possible blend configurations by performing light curve fits of our highest-quality follow-up photometry (data in the Sloan i band) following the procedures described by Torres et al. (2004). Briefly, we attempted to reproduce the observed photometric variations with a model based on the EBOP binary-fitting program (Etzel 1981; Popper & Etzel 1981) in which three stars contribute light, two of which form an eclipsing binary with the orbital period found for XO-5. The light from the third star (the candidate) then dilutes the otherwise deep eclipses of the binary, reducing them to the level observed for HTR176-002 (∼1.2% depth). The properties of the main star were adopted from the results of our analysis below, and those of the binary components (mass, size, brightness) were constrained to satisfy representative model isochrones. We explored all possible combinations for the binary components and determined the best fits to the light curve in a chi-square sense.

The case of a hierarchical triple (all stars at the same distance) yielded an excellent fit to the photometry (see the top curve in Figure 4), but implies an eclipsing binary with a primary that is half as bright as HTR176-002 itself. This is clearly ruled out by our Keck spectra and even our digital speedometer spectra, both of which would show obvious double lines.

We then considered scenarios in which the eclipsing binary is in the background (which would make it fainter), and is spatially unresolved. Because the proper motion of the candidate is relatively small (∼30 mas yr^{-1}; Monet et al. 2003), the chance alignment would remain very close for decades, precluding the direct detection of the binary in archival photographic images such as those available from the Digital Sky Survey. For convenience we parameterized how far behind the eclipsing binary is placed relative to the candidate in terms of the difference in distance modulus, Δm, and we explored a wide range of values. As an example, we find that for $\Delta m = 4$ (binary about 1.7 kpc behind) the best fit yields a relative brightness for the binary of only 5%, which is at or below our detection threshold of 5%–10% from the Keck spectra. However, the ingress and egress are clearly too long given the quality of our photometry (Figure 4, bottom curve). For a smaller separation of $\Delta m = 2$ (binary some 500 pc behind) the fit is somewhat better, though still visibly in disagreement with the observations (Figure 4, middle curve), and the relative brightness increases to 20%, which we would have noticed. Additional tests changing

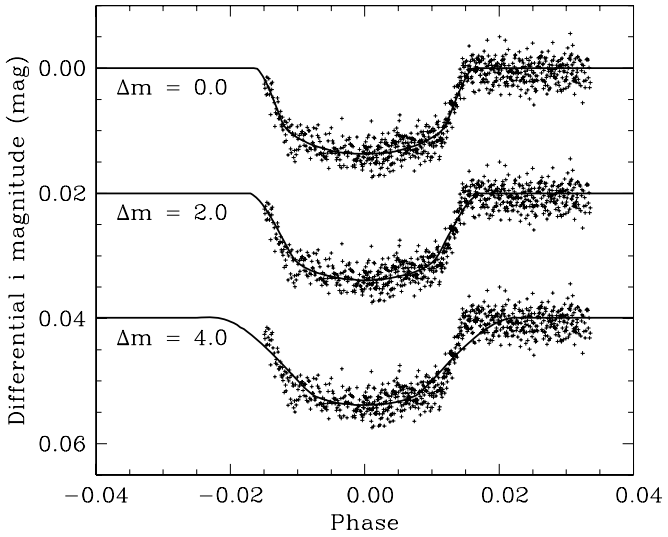

Figure 4. Blend modeling for XO-5, based on our Sloan i-band photometry. As examples we show the best fits corresponding to three different blend scenarios, with the bottom two displaced vertically for clarity. Top: model corresponding to a hierarchical triple (see the text), which is ruled out because the implied brightness of the eclipsing binary is so large (∼50%) that our spectra would be double-lined. Middle: model corresponding to a chance alignment with a background eclipsing binary, in which the distance modulus difference between the binary and the candidate is $\Delta m = 2$. The ingress and egress are already seen to be too long, and the fit implies a relative brightness of ∼20% that would be easily detectable spectroscopically. Bottom: chance alignment model with $\Delta m = 4$ in which the binary is much fainter (∼5%), but the best-fit model does not match the observations well. These simulations rule out background blend scenarios.

the inclination angle from the edge-on configurations considered above to lower angles did not alleviate the discrepancies.

The above modeling rules out both a hierarchical triple and a background eclipsing binary as possible alternate explanations for the photometric signals we detect. This, combined with the lack of any clear correlation between the bisector spans and the RVs, constitutes compelling evidence of the planetary nature of HTR176-002 = XO-5, and convinces us that the scatter in the bisector spans described above is intrinsic to the star.

5. ANALYSIS

In this section we describe briefly our analysis yielding the orbital, planetary, and stellar parameters for the XO-5 system.

5.1. Light Curve and Radial Velocity Analysis

For the initial characterization of the spectroscopic orbit, we fitted a Keplerian model to the Keck RV data, allowing for eccentricity by including as adjustable parameters the Lagrangian orbital elements $k = e\cos\varpi$ and $h = e\sin\varpi$, in addition to a velocity offset γ, the semi-amplitude K and the epoch E. The period P was held fixed at the value found from the HATNet light curve analysis (from BLS, see above). We found that k and h are insignificant compared to their uncertainties ($k = -0.003 \pm 0.029$, $h = -0.009 \pm 0.023$), suggesting that the orbit is circular. However, in the determination of the orbital and stellar parameters, we incorporated the uncertainties yielded by the k and h orbital elements.

We proceeded next with a joint fit using all data sets, namely, the HATNet discovery light curve, the FLWO 1.2 m follow-up light curves, and the Keck RVs along with the initial estimates of the spectroscopic properties derived through the SME analysis. The follow-up light curves were modeled using

Table 2
Stellar Parameters for XO-5

Parameter	Value	Source
$T_{\rm eff}$ (K)	5370 ± 70	SME[a]
[Fe/H]	+0.05 ± 0.06	SME
$v \sin i$ (km s^{-1})	0.7 ± 0.5	SME
$M_\star$ ($M_\odot$)	0.88 ± 0.03	Y^2+LC+SME[b]
$R_\star$ ($R_\odot$)	1.08 ± 0.04	Y^2+LC+SME
$\log g_\star$ (cgs)	4.31 ± 0.03	Y^2+LC+SME
$L_\star$ ($L_\odot$)	0.88 ± 0.09	Y^2+LC+SME
M_V (mag)	5.06 ± 0.12	Y^2+LC+SME
Age (Gyr)	14.8 ± 2.0	Y^2+LC+SME
Distance (pc)	260 ± 12	Y^2+LC+SME

Notes.
[a] SME' package for analysis of high-resolution spectra (Valenti & Piskunov 1996). See the text.
[b] Y^2+LC+SME = Yale–Yonsei isochrones (Yi et al. 2001), light curve parameters, and SME results.

Table 3
Orbital and Planetary Parameters

Parameter	Value
Light curve parameters	
P (days)	4.187757 ± 0.000011
E (BJD)	2454552.67168 ± 0.00029
T_{14} (days)[a]	0.1307 ± 0.0013
$T_{12} = T_{34}$ (days)[a]	0.0175 ± 0.0013
$\zeta/R_\star$ (d^{-1})	17.779 ± 0.091
$a/R_\star$	9.67 ± 0.35
$R_p/R_\star$	0.1050 ± 0.0009
$b \equiv a\cos i/R_\star$	$0.562^{+0.033}_{-0.052}$
i (deg)	86.7 ± 0.4
Spectroscopic parameters	
K (m s^{-1})	144.9 ± 2.0
$C_{\rm BS}$	0.125 ± 0.025
$C_{\rm S-index}$	0 (adopted)
$k \equiv e\cos\omega$	+0.008 ± 0.010
$h \equiv e\sin\omega$	+0.010 ± 0.013
Planetary parameters	
M_p ($M_{\rm J}$)	1.059 ± 0.028
R_p ($R_{\rm J}$)	1.109 ± 0.050
$C(M_p, R_p)$	0.23
ρ_p (g cm^{-3})	$0.96^{+0.14}_{-0.11}$
a (AU)	0.0488 ± 0.0006
$\log g_p$ (cgs)	3.33 ± 0.04
$T_{\rm eq}$ (K)	1221 ± 27
Θ	0.105 ± 0.005

Note.
[a] T_{14}, total transit duration, time between first and last contact; $T_{12} = T_{34}$, ingress/egress time, time between first and second, or third and fourth contacts.

the analytic formalism of Mandel & Agol (2002), assuming quadratic limb darkening. The limb darkening coefficients $\gamma_{1,z}$, $\gamma_{1,i}$, $\gamma_{2,z}$, and $\gamma_{2,i}$ were taken from Claret (2004), interpolating to the values provided by the initial stellar atmospheric analysis in Section 3.2. The adjusted parameters for the joint fit were $T_{\rm c,-270}$, the time of first transit center in the HATNet campaign, $T_{\rm c,20}$, the time of the transit center at the last follow-up (on 2008 March 26), m, the out-of-transit magnitude of the HATNet light curve in the I band, the semi-amplitude of the RV K, the velocity offset γ, the Lagrangian orbital elements k and h, the fractional planetary radius $p \equiv R_{\rm p}/R_\star$, the square of the impact parameter b^2, the quantity $\zeta/R_\star = (2\pi/P)(a/R_\star)(1-b^2)^{-1/2}\sqrt{1-e^2}(1+h)^{-1}$—which is related to the duration of the transit[11] as $T_{\rm dur} = 2(\zeta/R_\star)^{-1}$, and the out-of-transit magnitudes $m_{\rm c,0}, m_{\rm c,4}, m_{\rm c,9}$, and $m_{\rm c,20}$ for the four follow-up light curves. See Pál et al. (2008) for a detailed discussion about the advantages of this set of parameters. The initial values were based on the BLS analysis and our initial characterization of the orbit. To obtain the best-fit values, we utilized the downhill simplex algorithm (see Press et al. 1992). The uncertainties and the correlations were determined using the Markov Chain Monte Carlo method (Ford 2006) which yields the a posteriori distribution of the adjusted values.

As mentioned in Section 4, we found that there is a significant correlation between the RV residuals and the bisector spans. This suggests that it might be possible to improve the RV fit by including an additional term to account for this correlation. We therefore expanded the model for the velocity variation to

$$v_i = \gamma + K \cdot {\rm RV}_0\left(\frac{2\pi(t_i - E)}{P}, k, h\right) + C_{\rm BS} b_i \qquad (1)$$

where ${\rm RV}_0(\cdot,\cdot,\cdot)$ represents the *base* function for the RV variations[12] and b_i is the actual bisector span variation for the ith measurement. We found that when omitting the last term the unbiased residual is 8.8 m s^{-1}, whereas its inclusion leads to decreased residuals of 4.6 m s^{-1}, nearly a factor of 2 better. We also tested whether the inclusion of a similar term in Equation (1) proportional to the stellar activity index (with a coefficient $C_{\rm S\text{-}index}$) provides any further improvement in the fit, but found that it actually degrades the residuals slightly. The final orbital and planetary parameters (and their uncertainties) derived in this paper are based on the above-discussed RV model function decorrelated against the bisector variations.

5.2. Stellar and Planetary Parameters

The stellar parameters were determined in an iterative way as follows. As pointed out by Sozzetti et al. (2007), the stellar density is a better luminosity indicator than the spectroscopic value of $\log g_\star$. In a first-order approximation the density is related to the observable quantities P and $a/R_\star$ as $\rho_\star = (3\pi)G^{-1}P^{-2}(a/R_\star)^3$. We used the values of $T_{\rm eff}$ and [Fe/H] from the SME analysis, together with the distribution of $\rho_\star$ (derived from $a/R_\star$) to estimate the stellar parameters from the Yonsei–Yale evolution models, as published by Yi et al. (2001) and Demarque et al. (2004). This resulted in a posteriori distributions of those stellar parameters, including the mass, radius, age, luminosity, and colors. From the mass and radius distributions, we obtained a new value and uncertainty for the stellar surface gravity: 4.31 ± 0.03. Since this value is significantly smaller than the previous value based on the SME analysis (Section 3.2), we repeated the atmospheric modeling by fixing the surface gravity to the new value (4.31 ± 0.03), and allowing only the metallicity and effective temperature to vary. This next iteration of the SME analysis yielded $T_{\rm eff}$ = 5370 ± 70 K and [Fe/H] = +0.05 ± 0.06. Based on these new atmospheric parameters, the limb darkening coefficients were re-calculated and we repeated the joint fit for the light

[11] Here duration is not the total duration between the first and the last contact but defined as the interval between the instances when the center of the planet crosses the limb of the stars inward and outward.
[12] This function has three arguments: the mean longitude measured from the transit center and the two Lagrangian orbital elements k and h. It is easy to show that if $k = h = 0$, ${\rm RV}_0(\lambda, 0, 0) = -\sin(\lambda)$.

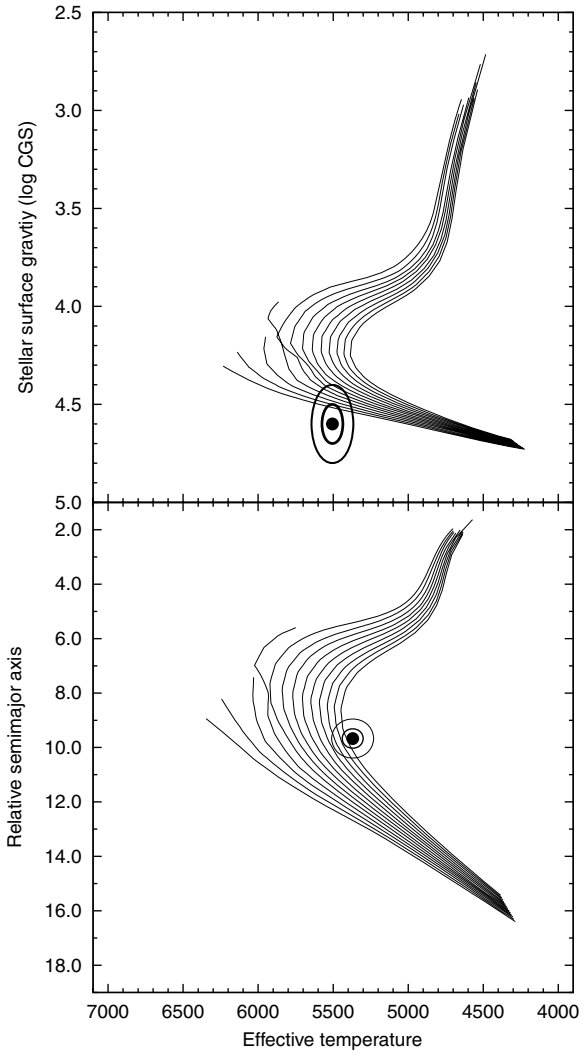

Figure 5. Stellar evolution isochrones from the Yonsei–Yale models, corresponding to ages between 2 and 14 Gyr (in steps of 1 Gyr), as a function of both surface gravity (top) and normalized semimajor axis $a/R_\star$ (bottom). In the top panel, the isochrone metallicity ([Fe/H] = +0.16), spectroscopic surface gravity, and temperature are from our initial SME analysis, the latter two shown with 1σ and 2σ confidence ellipsoids. In the lower panel, the metallicity ([Fe/H] = +0.05), temperature, and $a/R_\star$ are from the iterative analysis described in the text. Note that the latter quantities result in a significantly different evolutionary state for the star.

curve and RV parameters, followed by the stellar evolution modeling once again, in the same way as discussed earlier. In this iteration the surface gravity barely changed ($\log g_\star = 4.33 \pm 0.04$), so the stellar previous parameters were accepted as final (Table 2). In Figure 5, we plot the evolutionary isochrones as the function of the effective temperature and both the stellar surface gravity and $a/R_\star$ (these are used as luminosity indicators). The temperature, surface gravity, and relative semimajor axis values discussed here are also superimposed on these isochrone plots.

The results from this second global fit to all the available data (photometry, RVs) are listed in Table 3. In addition, values for some auxiliary parameters in this fit are $T_{c,-270} = 2453338.22311 \pm 0.00236$ (BJD), $T_{c,20} = 2454552.67174 \pm 0.00029$ (BJD), $m = 11.33042 \pm 0.00010$ mag, and the Keck velocity offset is $\gamma = 0.8 \pm 0.1$ m s^{-1}. The best-fit values and uncertainties for the fitted parameters are straightforward to obtain from the MC distributions. These, in turn, lead to the

Table 4
Individual Transit Center Measurements

Event	T_C(BJD)[a] (2,454,000+)	T_C(BJD)[b] (2,454,000+)
0	468.91868 ± 0.00181	468.91666 ± 0.00028
4	485.66932 ± 0.00058	485.66768 ± 0.00028
9	506.60475 ± 0.00057	506.60645 ± 0.00027
20	552.67152 ± 0.00041	552.67174 ± 0.00029

Notes.
[a] Derived frp, the individually fitted the transit centers, while the other light curve parameters were constrained to be equal.
[b] Derived by interpolation from the joint fit results, assuming a constant period.

planetary parameters and their uncertainties by using a direct combination of the a posteriori parameter distributions of the light curve, RV, and stellar parameters. We find that the mass of the planet is $M_p = 1.059 \pm 0.028\ M_J$, the radius is $R_p = 1.109 \pm 0.050\ R_J$, and its density is $\rho_p = 0.96^{+0.14}_{-0.11}$ g cm^{-3}. These quantities are also collected in Table 3. The correlation coefficient $C(M_p, R_p)$ between the planetary mass and radius is listed as well. We also estimated the individual transit centers of the four follow-up light curves, by adjusting only the light curve parameters ($R_p/R_\star$, b^2, $\zeta/R_\star$, out-of-transit magnitudes) while the transit centers were not constrained by a given epoch and period. We obtained that the individual transit centers do not differ significantly from the interpolated transit centers (derived from the results of the joint fit), i.e., the available data do not show any signs for transit timing variations. The independently fitted transit centers for the events $N_{tr} = 0$, $N_{tr} = 4$, and $N_{tr} = 20$ differ from the linearly interpolated values by less than 1.5σ, and the difference at the event $N_{tr} = 9$ is nearly 2.3σ. The independently fitted and the interpolated transit instants are shown in Table 4.

Using our best fit model, we also checked the amplitude of the out-of-transit variations of the HATNet light curve, by performing a Fourier analysis on the fit residuals. We found no significant variation in the stellar flux, and all Fourier amplitudes were less than 0.7 mmag. This estimation gives an upper limit for the stellar activity, and is in line with the small S values derived from spectroscopy ($S \lesssim 0.186$; see Table 1). It is somewhat surprising that in spite of the small activity based on the spectroscopic S index, the light curve out-of-transit variation and the low $v \sin i$ rotational velocity of the star, the bisector spans exhibit such a large scatter.

The Yonsei–Yale evolutionary models also provide the absolute magnitudes and colors for different photometric bands. We compared the $V - I$ model color with the observed TASS color (see Droege et al. 2006). Since $(V-I)_{YY} = 0.815 \pm 0.016$ and $(V-I)_{TASS} = 0.82 \pm 0.09$, we conclude that the star is not significantly affected by interstellar reddening (also note the Galactic latitude of XO-5, which is $b = 26.^\circ9$). Therefore, for the distance determination we use the distance modulus $V_{TASS} - M_V = 7.18 \pm 0.13$, which corresponds to $d = 260 \pm 12$ pc.

6. DISCUSSION

In this paper, we have described our independent detection of the transiting planet XO-5b using the HATNet observations. A significant component of our effort has been to examine possible astrophysical false positives and to model the data in detail in order to rule them out. In this way, we have provided new and crucial support for the planetary nature of the object.

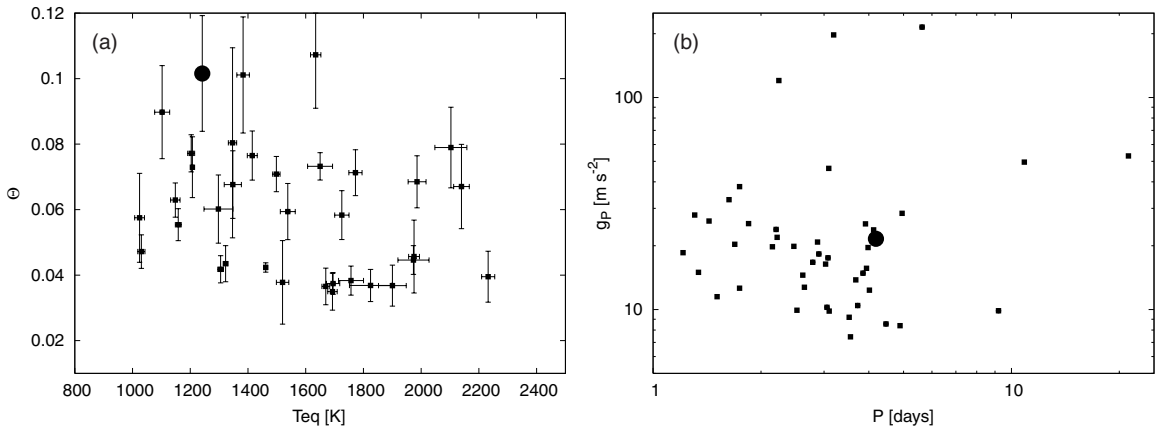

Figure 6. (a) Safronov number vs. equilibrium temperature for the known transiting extrasolar planets. XO-5b is marked with a larger dot and it is located at the upper envelope of the Class I distribution of planets (XO-5b > 0.05). (b) Surface gravities as the function of the orbital period for the known extrasolar planets. With its relatively high surface gravity and orbital period, XO-5b falls slightly off the main distribution.

We also present refined values for the system parameters. It is reassuring that the planetary parameters in B08 and this work are consistent within 1σ. This, however, is somewhat coincidental, since the stellar parameters are quite different. Based on our SME analysis, we derive a lower effective temperature ($T_{\rm eff}$ = 5370 ± 70 K as compared to 5510 ± 44 K in B08), and a lower metallicity ([Fe/H] = +0.05 ± 0.06 vs. 0.25 ± 0.03). The difference is attributed to our iterations on the SME analysis and the transit-fitting, using the $a/R_\star$ based mean stellar density as a luminosity indicator, and fixing the corresponding $\log g_\star$ in the SME analysis (i.e., solving only for [Fe/H] and $T_{\rm eff}$). We derive a smaller stellar mass: 0.88 ± 0.03 $M_\odot$ vs. 1.0 ± 0.03, $M_\odot$, based on the same Yi et al. (2001) isochrones. Due to the high precision photometric and RV data, we are able to refine the planetary and orbital parameters of the system, and decrease the uncertainties typically by a factor of ∼2–3.

Based on the models of Liu et al. (2008), after re-scaling the semimajor axis to match the insolation flux XO-5b would have if it orbited a G2V dwarf ($a_{\rm equiv}$ = 0.05313 AU), the measured mass and radius of XO-5b require a small core to be consistent with theory even if no internal heating is assumed. Using the work of Fortney et al. (2007), XO-5b is consistent with a 300 Myr old planet with a 50 $M_\oplus$ core, a 1 Gyr old planet with a 25 $M_\oplus$ core, or a 4.5 Gyr planet with a core smaller than 10 $M_\oplus$ mass. The incident flux on XO-5b is $\sim 4.83 \times 10^8$ erg s^{-1} cm^{-2}. This corresponds to a pL class planet, based on the definitions of Fortney et al. (2008), although it falls fairly close to the transition area between the pL and pM classes.

We confirm that the planet has a remarkably high Safronov number, $\Theta \equiv 1/2(V_{\rm esc}/V_{\rm orb})^2 = 0.105 \pm 0.005$, placing it at the high end of the Class I planets as defined by Hansen & Barman (2007). The plot of the Safronov numbers for the known TEPs as a function of the equilibrium temperature is displayed in Figure 6(a). We also confirm that XO-5b has an anomalously high surface gravity, as compared to other TEPs with similar period (Southworth et al. 2007).

Altogether, XO-5 appears to be an interesting system exhibiting a number of anomalies including non-trivial bisector span variations, and anomalously high Safronov number and surface gravity. Future observations and theoretical work are required to understand these properties.

HATNet operations have been funded by NASA grants NNG04GN74G, NNX08AF23G and SAO IR&D grants. Work of G.Á.B. was supported by the Postdoctoral Fellowship of the NSF Astronomy and Astrophysics Program (AST-0702843). We acknowledge partial support also from the Kepler Mission under NASA Cooperative Agreement NCC2-1390 (D.W.L., P.I.). G.K. thanks the Hungarian Scientific Research Foundation (OTKA) for support through grant K-60750. A.P. is grateful for the SAO Visiting Student Fellowship that supported his work. This research has made use of Keck telescope time granted through NASA and NOAO (programs N162Hr, N128Hr, and A264Hr).

REFERENCES

Alonso, R., et al. 2004, ApJ, 613, L153
Bakos, G. Á., Lázár, J., Papp, I., Sári, P., & Green, E. M. 2002, PASP, 114, 974
Bakos, G. Á., Noyes, R. W., Kovács, G., Stanek, K. Z., Sasselov, D. D., & Domsa, I. 2004, PASP, 116, 266
Bakos, G. Á., et al. 2007, ApJ, 670, 826
Bakos, G. Á., et al. 2009, ApJ, 696, 1950
Brown, T. M. 2003, ApJ, 593, L125
Brown, T. M., & Charbonneau, D. 2000, in ASP Conf. Ser., Disks, Planetesimals, and Planets, ed. F. Garzón et al. (San Francisco, CA: ASP), 584
Burke, C. J., et al. 2007, ApJ, 671, 2115
Burke, C. J., et al. 2008, ApJ, 686, 1331
Butler, R. P., Marcy, G. W., Williams, E., McCarthy, C., Dosanjh, P., & Vogt, S. S. 1996, PASP, 108, 500
Claret, A. 2004, A&A, 428, 1001
Cameron, A. C., et al. 2007, MNRAS, 375, 951
Demarque, P., Woo, J.-H., Kim, Y.-C., & Yi, S. K. 2004, ApJS, 155, 667
Droege, T. F., Richmond, M. W., & Sallman, M. 2006, PASP, 118, 1666
Dunham, E. W., Mandushev, G. I., Taylor, B. W., & Oetiker, B. 2004, PASP, 116, 1072
Etzel, P. B. 1981, Photometric and Spectroscopic Binary Systems (Dordrecht: Reidel), 65
Ford, E. 2006, ApJ, 642, 505
Fortney, J. J., Lodders, K., Marley, M. S., & Freedman, R. S. 2008, ApJ, 678, 1419
Fortney, J. J., Marley, M. S., & Barnes, J. W. 2007, ApJ, 659, 1661
Hansen, B. M. S., & Barman, T. 2007, ApJ, 671, 861
Horne, K. 2001, in 4th Annual ROE Workshop, Techniques for the Detection of Planets and Life beyond the Solar System, ed. W.R.F. Dent (Edinburgh, Scotland: Royal Observatory), 5
Kovács, G., Bakos, G. Á., & Noyes, R. W. 2005, MNRAS, 356, 557
Kovács, G., Zucker, S., & Mazeh, T. 2002, A&A, 391, 369
Latham, D. W. 1992, in ASP Conf. Ser. 32, IAU Coll. 135, Complementary Approaches to Double and Multiple Star Research, ed. H. A. McAlister & W. I. Hartkopf (San Francisco, CA: ASP), 110
Liu, X., Burrows, A., & Ibgui, L. 2008, ApJ, 687, 1191
Mandel, K., & Agol, E. 2002, ApJ, 580, L171
Mandushev, G., et al. 2007, ApJ, 667, L195
Marcy, G. W., & Butler, R. P. 1992, PASP, 104, 270
McCullough, P. R., Stys, J. E., Valenti, J. A., Fleming, S. W., Janes, K. A., & Heasley, J. N. 2005, PASP, 117, 783
McCullough, P. R., et al. 2006, ApJ, 648, 1228

Monet, D. G., et al. 2003, AJ, 125, 984
Noyes, R. W., Hartmann, L. W., Baliunas, S. L., Duncan, D. K., & Vaughan, A. H. 1984, ApJ, 279, 763
Pál, A., & Bakos, G. Á. 2006, PASP, 118, 1474
Pál, A., et al. 2008, ApJ, 680, 1450
Pollacco, D., et al. 2006, PASP, 118, 1407
Popper, D. M., & Etzel, P. B. 1981, AJ, 86, 102
Press, W. H., Teukolsky, S. A., Vetterling, W. T., & Flannery, B. P. 1992, Numerical Recipes in C: The Art of Scientific Computing (2nd edn.; Cambridge: Cambridge Univ. Press)
Queloz, D., et al. 2001, A&A, 379, 279
Shporer, A., Mazeh, T., Moran, A., Bakos, G., Kovacs, G., & Mashal, E. 2006, in Tenth Anniversary of 51 Peg-b: Status of and Prospects for Hot Jupiter Studies, ed. L. Arnold, F. Bouchy, & C. Moutou (Paris: Frontier Group), 196
Shporer, A., et al. 2009, ApJ, 690, 1393
Southworth, J., Wheatley, P. J., & Sams, G. 2007, MNRAS, 379, 11
Sozzetti, A., et al. 2007, ApJ, 664, 1190
Street, R. A., et al. 2003, in ASP Conf. Ser. 294, Scientific Frontiers in Research on Extrasolar Planets, ed. D. Deming & S. Seager (San Francisco, CA: ASP), 405
Torres, G., Konacki, M., Sasselov, D. D., & Jha, S. 2004, ApJ, 614, 979
Torres, G., Konacki, M., Sasselov, D. D., & Jha, S. 2005, ApJ, 619, 558
Torres, G., et al. 2007, ApJ, 666, 121
Valenti, J. A., & Fischer, D. A. 2005, ApJS, 159, 141
Valenti, J. A., & Piskunov, N. 1996, A&AS, 118, 595
Vogt, S. S., et al. 1994, Proc. SPIE, 2198, 362
West, R. G., et al. 2008, A&A, submitted (arXiv:0809.4597)
Yi, S. K., et al. 2001, ApJS, 136, 417